The Importance of Liquid Compressibility in Calculations of Fluid Dynamics Inside a DOD Piezoelectric Ink Jet Nozzle

E. Magen and M. Gottlieb*

Chemical Engineering Department, Ben Gurion University of the Negev, Beer Sheva, Israel

This study is aimed at determining the effect of the minute liquid compressibility on the flow of ink in a piezo-diaphragm driven Drop-On-Demand (DOD) ink jet nozzle. This goal is achieved by a comparison between the results obtained numerically for compressible and incompressible flows by means of Computational Fluid Dynamics calculations. In these calculations the exact geometry of the entire flow channel is modeled. Significant differences between the two flow models are observed in many aspects of the flow and drop evolution characteristics. Also, in some cases, seemingly similar features have been found to result from different physical driving forces. Despite the low Mach number and low condensation values involved, the very slightly compressible flow and the incompressible flow are very different. It is concluded that acoustic effects cannot be ignored and the incorporation of ink compressibility in the physical analysis of this flow system is essential.

Journal of Imaging Science and Technology 48: 335–341 (2004)

Introduction

It is common practice in fluid dynamics modeling and calculations to assume that unless exposed to extremely high pressures, liquids are practically incompressible. The incompressibility assumption results in substantial simplification of the governing equations allowing solution of otherwise intractable problems. Published investigations of the fluid dynamics in drop-on-demand (DOD) piezoelectric ink jet devices differ in their attitude towards the importance of ink compressibility in defining the physical behavior of the liquid inside the nozzle. Some researchers follow common practice and completely ignore liquid compressibility in their flow models[1] or simulations.[2] Others[3–6] assign a great deal of importance to the ink's minute compressibility and consequential acoustic effects. Dimensional analysis, which is often useful in identifying the important physical features in a given system, yields inconclusive results in this case, as will be demonstrated below. Thus, it is impossible to reach a conclusion regarding the importance of ink compressibility in the operation of DOD piezoelectric ink jet nozzles without undertaking a comprehensive study of this issue.

Experimental studies of the flow in piezoelectric ink jet nozzles are extremely difficult due to the highly transient nature of the flow as well as to the miniature and complex geometry of the flow channel. The high speed, transient flow and the complex boundary conditions limit the possibility for analytical solutions for the flow field. Thus, a numerical approach to the modeling of the system is the only viable alternative to obtain pressure and velocity distribution data not readily available from experiments. Yet, a numerical solution depends on the physical model prescribed to the system and once again one is faced with the question whether compressibility effects should be taken into account. Incorporation of liquid compressibility into the model imposes a major burden on the numerical scheme and requires extensive computational resources. Hence, resolution of this issue should provide a great service for future research.

The objective of this study is to present a detailed study of the effect of the minute compressibility of ink on the fluid behavior in DOD devices. This is achieved by comparing the behavior of compressible and incompressible liquids in the course of drop formation in a commercial piezo-diaphragm ink jet nozzle. More specifically, we compare the instantaneous internal pressure distribution and meniscus perturbations during short time intervals calculated numerically for these two types of liquids. To carry out these calculations use was made of a Computational Fluid Dynamics (CFD) software package based on the Finite Element Method.[7] This investigation also allows us to fully appreciate the importance of acoustics in these systems.

Nozzle Description and Theoretical Framework

A cross-section of a single commercial piezo-diaphragm nozzle, designed and manufactured by Aprion (Aprion Digital Ltd, Netanya 42505, Israel) is shown in Fig. 1. The nozzle consists of two cylindrical hollow tubes removed from a porous metal, which wraps the ink

Original manuscript received September 24, 2003

* Moshe@inca.bgu.ac.il; fax: +972.8.647.2916

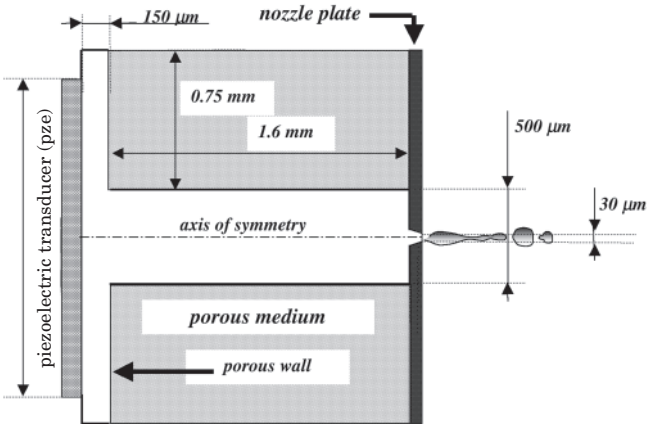

Figure 1. Details of the Aprion DOD ink jet nozzle.

chamber and enables flow of ink into or out of the ink reservoir. The circular piezoelectric transducer (pze) is located opposite to the nozzle exit at the back-end of the flow channel. A detailed description of the nozzle geometry is given elsewhere.[8,9]

The voltage applied to the pze triggers its deformation. Upon deformation, the pze arches into or out of the ink cavity, and subsequently ejects a drop of ink with a typical velocity of ~10 m/s. The applied voltage is a rectangular pulse with a typical duration of T_2 = 2–5 μs, and a drop ejection cycle T_1 > 10 μs (or single nozzle jetting frequency <100 kHz). Measurements carried out in Aprion laboratories revealed that the deformation rise time of the pze is approximately 1 μs.[10] The following values have been selected to represent the water based ink: $\rho_0 = 10^3$ Kg/m^3 for the equilibrium density, $\sigma = 0.03$ N/m for the surface tension, and $\mu = 10^{-2}$ Pa•s for ink viscosity.

Based on a dimensional analysis in which nozzle diameter and drop velocity were used for characteristic length and velocity, respectively, it was concluded that the flow is laminar, surface tension forces are probably of importance, and gravitational forces are negligible. Despite the low Reynolds number, inertial forces are not ignored in view of the large acceleration of the meniscus during drop formation.[8,9]

As already mentioned, we will attempt to estimate the importance of liquid compressibility by dimensional analysis. Although volume changes in liquids are generally negligibly small, the very fast pze deformation (Δt~1μs) inside the small ink chamber may result in non-negligible acoustic effects.

For small density fluctuations in liquids, a linear relationship may be written between the acoustic pressure p, i.e., the gauge pressure which is the excess pressure above the reference equilibrium pressure, and the local change in density[11]:

$$p = (\rho - \rho_0)C^2 = s\rho_0 C^2 \tag{1}$$

Here ρ_0 is the equilibrium density, ρ is the instantaneous density, C is the speed of sound in the medium, and s is the condensation (defined as the relative change in density $s = (\rho - \rho_0)/\rho_0 = \Delta\rho/\rho_0$).

In general, we consider "incompressibility" a good approximation for a given flow when the condensation is much smaller than unity. In steady flows, the maximum change in pressure can be estimated from the stagnation pressure:

$$p = \rho_0 u^2 \tag{2}$$

where u is the fluid velocity.

Insertion into Eq. (1) results in the following expression for the condensation:

$$s = (u/C)^2 = Ma^2 \tag{3}$$

Hence, in a steady flow the incompressibility assumption is valid if the liquid velocity is much smaller than the speed of sound in the liquid:

$$Ma = u/C << 1 \tag{4}$$

Here Ma is the Mach number. The Mach number delineates three flow regimes: For $Ma \geq 1$ the ultrasonic flow system is subjected to shock waves and for $Ma << 1$ the flow is considered incompressible. The intermediate regime in which $Ma < 1$ but is not much smaller than unity is the compressible flow regime. Obviously, the determination of the border line between "smaller" and "much smaller" than unity is somewhat arbitrary and depends on the specifics of the flow system.

For the estimation of the maximum change in pressure in a transient flow, let us consider the following case: A piston with a cross sectional area A, accelerates from rest to a velocity u within a time interval of Δt in a pipe of length L filled with an inviscid fluid. Using Newton's second law we may write an expression for the pressure:

$$p = \frac{\Sigma F}{A} = \rho_0 L \frac{u}{\Delta t} \tag{5}$$

By equating Eqs. (5) and (1), we obtain the following expression for the condensation:

$$s = \frac{L}{C^2}\frac{u}{\Delta t} = (\frac{L}{C\Delta t})Ma \tag{6}$$

Thus, in the case of unsteady flow, the incompressibility assumption is valid if two conditions are satisfied: (i) $Ma << 1$ as stated by Eq. (4); (ii) The distance traveled by the sound wave during the characteristic time interval Δt, should be much larger than the dimensions of the flow system, L:

$$\frac{L}{C\Delta t} << 1 \tag{7}$$

Unless the latter condition is met the propagation of pressure changes along the flow system may not be considered instantaneous relative to the time interval Δt. As result, acoustic effects cannot be ignored and liquid compressibility should be considered.[14]

In order to assume ink compressibility for the transient flow inside a DOD nozzle, the conditions specified by Eqs. (4) and (7) or by Eq. (6), should be satisfied. Using the drop velocity as the characteristic velocity of the ink and taking C = 1500 m/s (close to the speed of sound in water at 20°C and atmospheric pressure[11]) we may obtain an estimate for the Mach number, Ma ~

0.007 << 1. To evaluate the second condition we use the pze characteristic time of deformation (~ 1 μs) as the representative time interval over which the flow changes significantly. It results in: $L/(C\Delta t) \sim 1.2$, which implies that the distance traveled by a sound wave during the time required for pze deformation is of the order of the ink chamber length. Hence, pressure propagation in the ink chamber as result of the pze deformation cannot be considered instantaneous. Yet, if we use these values in Eq. (6) we find that the condensation s << 1, which should justify the use of the incompressibility assumption. Thus, we are unable to either support or refute the incompressibility assumption due to the ambiguous results obtained from the dimensional analysis.

The behavior of this laminar Newtonian ink jet ejection system is governed by the equation of motion and the equation of continuity.[12] As may be appreciated from Fig. 1, the symmetry axis of the cylindrical flow channel can be used to reduce the problem into a 2-dimensional (2D) axisymmetric problem. Thus, in this work we solve the 2D axisymmetric laminar flow of a (1) slightly compressible and (2) incompressible, Newtonian liquid taking into account inertial and surface tension effects.

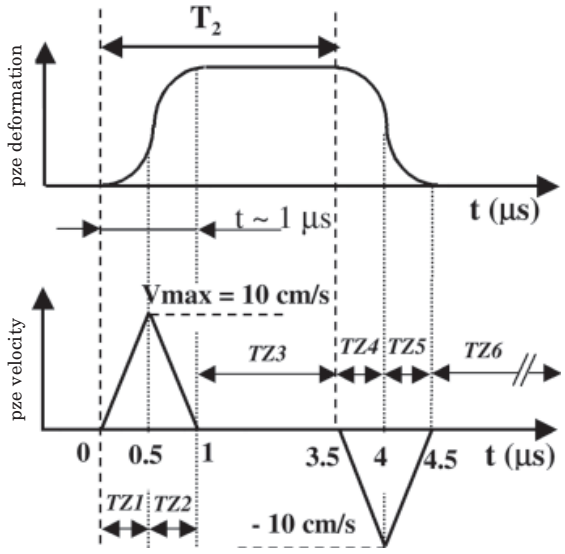

Figure 2. Deformation and velocity of the piezoelectric transducer wall in the axial direction and the definition of time zones (TZ).

The Computational Set-up

The fluid dynamics computations, were performed by means of a CFD commercial package POLYFLOW 3.6.0 (Polyflow S.A., Louvain-La-Neuve, Belgium), which employs the finite element method.[7] The details of the computational scheme and its implementation in this problem are described in great detail elsewhere.[8,9] Here we only give a brief outline of its salient features.

The computer representation of the system geometry is based on a cylindrical coordinate system with its origin positioned on the symmetry axis at the nozzle exit plane. Negative z values refer to distances upstream from the nozzle exit. The following boundary conditions (BC) have been used to describe the system:

1. *Solid walls*. "No slip" BC at solid walls: tangential velocity $V_s = 0$ and normal velocity $V_n = 0$.
2. *Axis of symmetry*. Symmetry BC: shear stress $\tau_s = 0$ and $V_n = 0$.
3. *The porous wall*. The porous medium, which wraps the ink chamber, is not included in the modeled geometry and is replaced by a "thin" (1D) porous wall boundary, which allows flow in and out of the ink chamber. The numerical implementation of this boundary condition comprises of a zero tangential velocity component ($V_s = 0$) along with a Darcy-like linear relationship between the normal stress (τ_n) and the normal velocity at the boundary:[13]

$$\tau_n = (\mu L_p/k_p)V_n \qquad (8)$$

   where μ is the viscosity of the fluid, L_p (= 2 mm) and k_p (= 2×10^{-12} m^2) are the thickness and permeability of the porous wall, respectively.
4. *Free surface*. The interfacial normal stress (τ_n) is equated to the sum of the outer pressure, P_0, and the capillary pressure.

$$\tau_n = P_0 + 2R/\sigma \qquad (9)$$

Here R is the Gaussian curvature of the surface and is a part of the flow solution. The outer pressure is set to zero, turning the calculated pressure into acoustic (gauge) pressure. The kinematic condition for the moving free-surface states that it must follow material points in the normal direction at all times, i.e., no mass flux across it.[13]

5. *The pze wall*. The response of the pze to a rectangular voltage pulse with a duration of T_2 = 3.5 μs, is represented by a symmetric sigmoidal deformation function with rise and decay times of 1 μs each, as depicted in Fig. 2. The pze wall BC is defined by means of the velocity function obtained from the time derivative of the deformation function rather than by the deformation function itself. *Vmax*, the maximum pze wall velocity, is assigned the value 10 cm/s required to reproduce the experimentally observed average meniscus velocity of 10 m/s.

For the sake of convenience in subsequent discussion, the pze wall velocity function was divided into six "time zones" (*TZ*). *TZ1* and *TZ2* correspond to the forward stroke of the pze wall. The time interval between the forward and backward strokes of the pze wall (zero velocity and maximum deformation) is labeled *TZ3*. The backward stroke of the pze wall into its original position occurs during *TZ4* and *TZ5*. Once returned to its original position, the pze wall is at rest (zero velocity and zero deformation) during *TZ6* until the next pulse is applied. The initial time $t = 0$, corresponds to the initial rise of the pze wall and is the reference time for all the results discussed here. It should be noted that the pze wall may experience additional deformation as result of the pressure reflection from the nozzle exit onto it. Due to the extremely small volume change even at its largest applied voltage, changes due to back pressure will not affect significantly the velocity pattern of the pze wall itself as shown in Fig. 2. Yet, deformation of the pze wall under the reflected pressure may alter subsequent pressure reflections at longer times and the resulting flow field near the back wall of the ink chamber. These effects have not been studied here and may merit further examination in the future.

To prevent divergence of the numerical scheme the maximum time step used in the numerical solution in view of the dimensions of the elements and the speed of sound, is set to 0.01 μs. For the compressible ink model

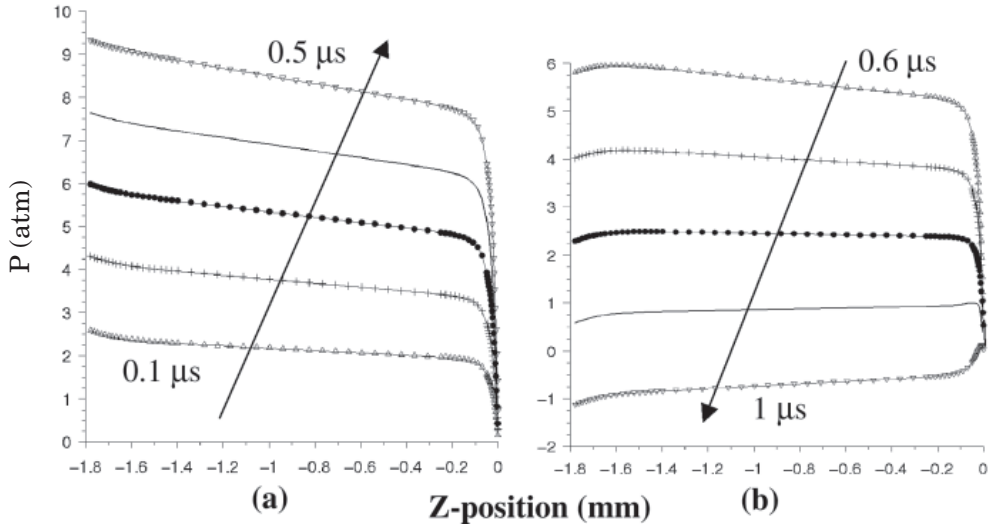

Figure 3. Incompressible flow. Pressure along the symmetry axis for times between (a) t = 0.1 – 0.5 μs (*TZ1*), and (b) 0.6 – 1 μs (*TZ2*), Δt = 0.1 μs. Time increases in the direction of the arrow.

the instantaneous ink density, ρ, is related to the pressure field p, by Eq. (1), whereas for the incompressible ink model the density is maintained at a constant value equal to the equilibrium density, ρ_0.

Numerical Results

In what follows we compare the results obtained for compressible and incompressible flows. Initially we compare the evolution of pressure inside the flow chamber during the pze forward stroke. Yet, since the objective of a DOD ink jet nozzle is to generate drops, most of the comparison is dedicated to the differences in the evolution of drop formation. To capture the features in this highly transient flow, the results are presented at time intervals of 0.1 μs. These time intervals should not be confused with the computation time-steps which are always smaller than 0.01 μs.

Figure 3 depicts the pressure values in an incompressible liquid along the symmetry axis at different times from 0.1 to 1.0 μs with a 0.1 μs interval, throughout the forward stroke of the pze (time zones *TZ1* and *TZ2*). In this and in subsequent figures the pze wall is positioned at the extreme left (z = –1.8 mm), and the nozzle exit at the extreme right (z = 0). We have shown elsewhere[8,9] that with few exceptions, symmetry axis pressure values provide good representation of the pressure in the flow channel. The increase in velocity (during *TZ1*) is accompanied by pressure increase (Fig. 3(a)), whereas the decrease in velocity (during *TZ2*) is accompanied by pressure decrease (Fig 3(b)). In both cases the pressure drop along the ink chamber (axial direction) is very moderate and most of the time it is limited to less than 1 atm. A notable exception is observed at close proximity to the nozzle exit section, in which the pressure drops to zero as imposed by the free surface boundary condition leading to large pressure gradients at the nozzle exit. At t = 0.1 μs the maximum pressure, located on the pze wall, already attained a value of 2.7 atm. Subsequently, the pressure increases at a constant rate of ~ 20 atm/μs reaching its maximum value of 9.5 atm still at the pze wall. This maximum is achieved at t = 0.5 μs which corresponds to the end of *TZ1* the time at which the pze wall reaches its maximum velocity *Vmax*. At the onset of wall deceleration at times corresponding to *TZ2*, pressure values (depicted in Fig. 3(b)) drop dramatically reaching a minimum value of –1.1 atm (gauge) on the pze wall at t = 1 μs. Also, the maximum value in the pressure is no longer at the pze wall shifting to the right with time.

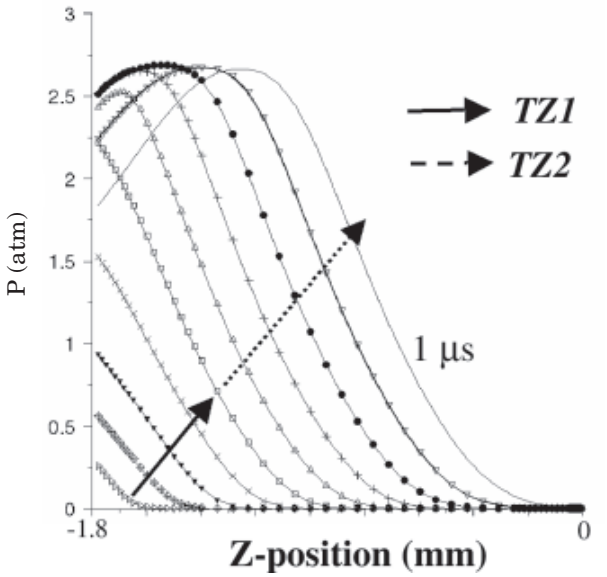

Figure 4. Compressible flow. Pressure along the symmetry axis for times between t = 0.1 – 1 μs (*TZ1* and *TZ2*, Δt = 0.1 μs). Time increases in the direction of the arrow.

Figure 4 depicts the pressure profile along the symmetry axis for a compressible flow. The time here varies between 0.1 – 1 μs as well, corresponding to time zones *TZ1* and *TZ2* (forward stroke) with intervals of 0.1 μs. It can be seen that the pressure builds up gradually next to the transducer, and propagates towards the nozzle exit with a fairly steep axial pressure gradient throughout the flow channel. The pressure on the pze wall increases with time until t ~ 0.5 μs (end of *TZ1*), paralleling the linear increase in the velocity at *TZ1*. The pressure peaks at 2.7 atm almost at the same time *Vmax* is reached. This is followed by a moderate decrease in pressure on the pze wall down to a value of 1.75 atm, reached at t = 1 μs. As the pressure wave propagates towards the nozzle exit, it maintains its peak value.

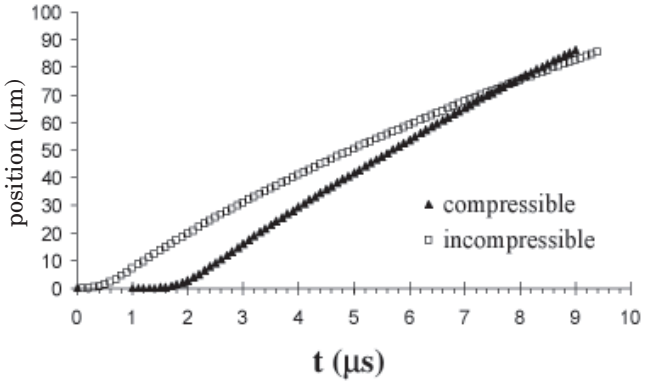

Figure 5. The protrusion of the meniscus tip versus time. Comparison between compressible and incompressible flows.

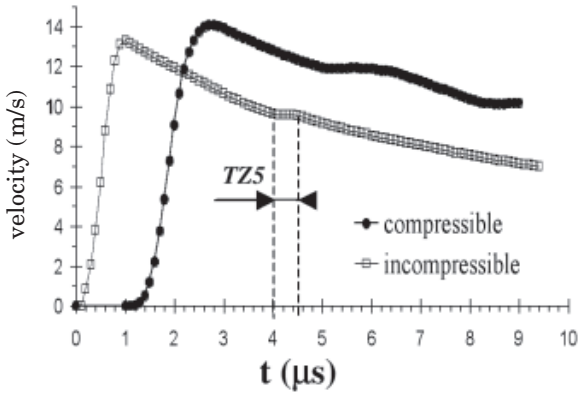

Figure 6. Time evolution of the meniscus-tip velocity for compressible and incompressible flows.

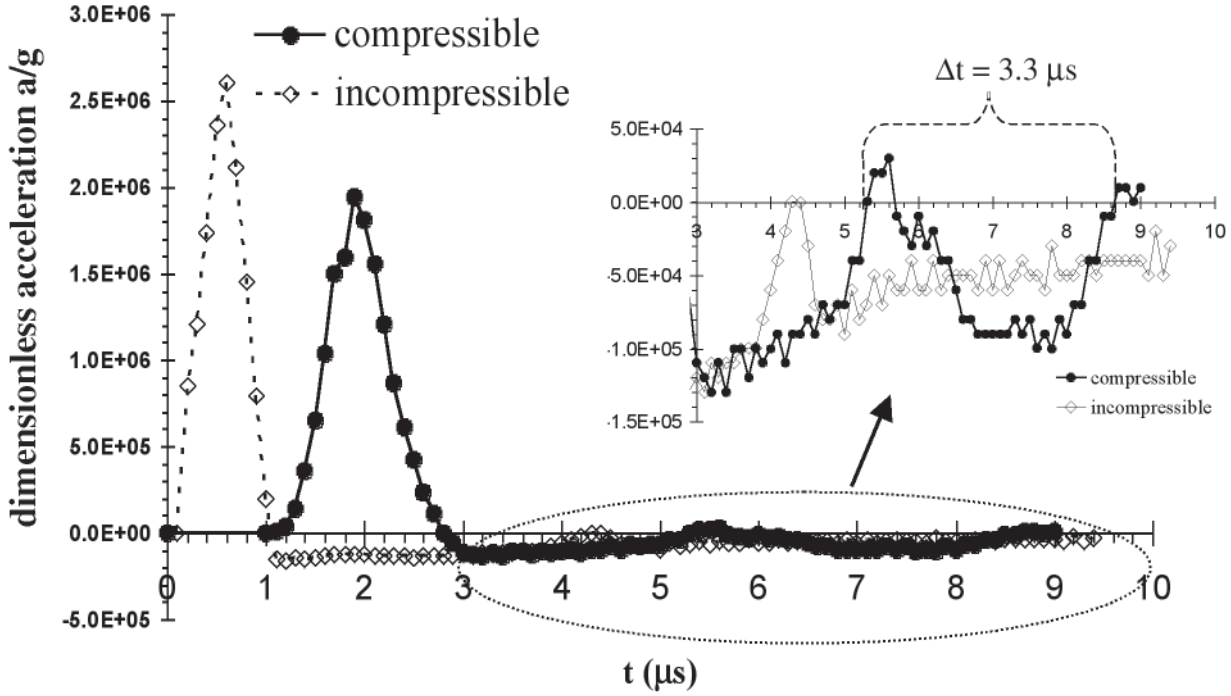

Figure 7. Acceleration of the meniscus tip vs. time for compressible and incompressible flows.

In Fig. 5 the calculated extent of protrusion of the meniscus tip as a function of time is shown for compressible and incompressible flows. For the compressible flow, there is a lag of 1.7 μs between the onset of motion of the pze wall and a discernable motion at the meniscus tip. For the incompressible flow, the motion of the meniscus tip is nearly instantaneous (0.4 μs). In both cases, the meniscus reaches a distance of three nozzle diameters (85 μm) from the nozzle exit after approximately 9 μs. The calculations were not pursued beyond this time (~ 9 μs), due to significant distortion of the mesh elements at the nozzle exit region.

By taking the time derivative of the meniscus tip position we have obtained the meniscus tip velocity shown in Fig. 6. Tip velocity provides a more sensitive discrimination between the features of compressible and incompressible flows. In the case of compressible flow, the velocity of the meniscus tip is zero for times shorter than 1.2 μs. For times longer than 1.2 μs, the meniscus tip accelerates until it reaches its maximum velocity (14 m/s) within 1.5 μs from the onset of its motion or 2.7 μs from the onset of the pze pulse. At this point, the velocity starts to decelerate moderately to a value of 10 m/s as $t \rightarrow 9$ μs. Still, the decrease in velocity is not completely monotonous and shows some waviness. For the incompressible flow, the meniscus reaches a slightly lower maximum velocity value of 13 m/s within 1 μs from the onset of the pze pulse. It then decreases moderately to a value of 7 m/s as $t \rightarrow 9$ μs with a single prominent interruption during *TZ5*.

From the time derivative of the velocity of the meniscus tip we have obtained its acceleration (Fig. 7). Considerable amount of "noise" is discernible in this figure as result of the inherent inaccuracies involved with numerical differentiation.

In the case of the compressible flow, the meniscus tip starts to accelerate at $t = 1$ μs, reaching its maximum acceleration value of 2×10^6 g at $t = 1.9$ μs (within *TZ3*),

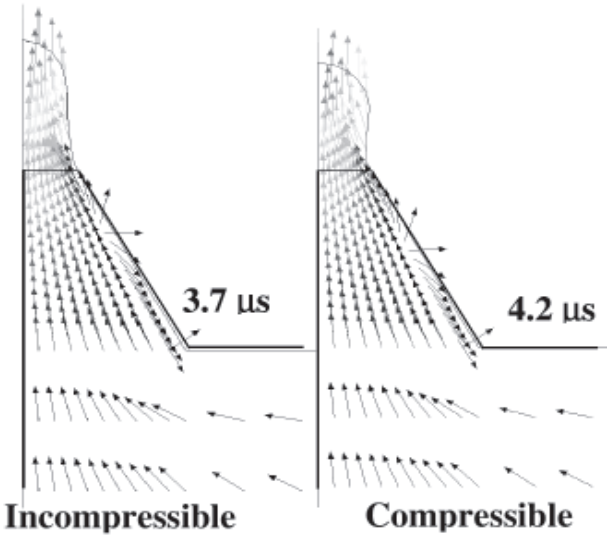

Figure 8. Onset of flow reversal at the tapered exit section of the nozzle for compressible (t = 4.2 μs) and incompressible (t = 3.7 μs) flows. The magnitude of the velocity vectors is indicated by their shading from black (lowest velocity) to gray (highest velocity).

and at t = 2.8 μs, the meniscus tip starts to decelerate. Intermittently, it gains relatively minor positive acceleration values of 3×10^4 g and 1×10^4 g at t = 5.3 μs and 8.6 μs respectively (Δt = 3.3 μs, both in *TZ6*). For the incompressible flow the meniscus tip accelerates almost instantaneously reaching a maximum value of 2.6×10^6 g at t = 0.6 μs. For times past 1.1 μs, the meniscus tip decelerates, with one exception occurring during *TZ4* and *TZ5*.

Inspection of the changes in the velocity field taking place in the nozzle exit region reveals that the meniscus acceleration induces suction of ink towards the exit plane from its adjacent surroundings. This behavior is observed for the compressible[8] as well as the incompressible flow. In the case of incompressible flow, the induced suction affects the entire ink chamber and the flow field is directed everywhere towards the nozzle exit. In contrast, for the compressible flow the suction induced by the drop is opposed by the pressure and flow reflections from walls and boundaries acting in the opposite direction.[8] Yet, in the tapered section the flow patterns are qualitatively similar for both models as shown in Fig. 8. The uniformly directed flow toward the exit at the tapered section of the nozzle is interrupted by the reversal of the flow field setting in near the wall of the tapered section (25 μm from the nozzle exit). The onset of flow reversal is first observed at t = 4.2 μs for compressible flow and at t = 3.7 μs for incompressible flow (see Fig. 8). At this point most of the ink in the vicinity of the nozzle plate flows outwards following the meniscus motion with a small portion of the liquid at a certain point near the walls flowing inwards. With time the extent of the inwards-flow zone increases in size, expanding towards the drop base and towards the center line and eventually it leads to formation of a bifurcation plane between the drop and the bulk of the ink.

Discussion

The results shown above clearly demonstrate the large differences in flow behavior resulting from the incorporation of acoustic effects. This is despite the fact that for 10 atm, the maximum pressure variation in our flow system, density variation (cf. Eq. 1) is at most 0.5 kg/m^3 which is equivalent to 0.05% of the liquid equilibrium density.

For incompressible flow as expected, the pressure in the ink chamber builds up instantaneously and almost uniformly. The maximum pressure is four times higher than that observed near the pze wall in compressible flow, in which the pressure builds up gradually and propagates with time toward the nozzle exit. The fourfold decrease in pressure values for the compressible flow cannot be fully attributed to the minor compressibility of the ink although some of the pze impact energy is probably absorbed by ink compression. The main source for the difference in pressure values stems from the fact that in the incompressible flow the mechanical energy is transferred instantaneously to the exit wall giving rise to the pressure surge. The magnitude of the pressure is in par with values estimated from a simple macroscopic mechanical energy balance.[12] Whereas, in the compressible flow the time it takes the mechanical energy or the velocity (cf. Figs. 4 and 6) fronts to reach the exit plane and the associated relatively large axial pressure (and hence velocity) gradients allow for additional dissipation of the mechanical energy.

In the case of compressible flow, strong coupling is found[8,9] between the pressure reflections at the nozzle plate end and the meniscus acceleration. The meniscus accelerates exactly at the instant the pressure wave arrives at the meniscus, and reaches its maximum acceleration value at the same time the reflected pressure reaches its peak value (t ~ 1.8 μs). This is also partially true for the incompressible flow: the meniscus starts accelerating at the onset of pze deformation since pressure propagation in incompressible flow is instantaneous, and the maximum acceleration is related to maximum pressure. Yet, time and magnitudes of these features vary between the two flows.

The evolution of meniscus acceleration depicted in Fig. 7 shows qualitatively similar features for both types of flows in the form of small bursts of acceleration in the deceleration region past the large acceleration peak: in the compressible flow they occur at t = 5.3 and 8.6 μs (*TZ6*) and in the incompressible flow at t = 4.3 μs (*TZ5*). Yet, despite the superficial similarity between the two models, the physical mechanism responsible for these features is very different. In the case of compressible flow the small bursts of meniscus acceleration were found to be related to secondary pressure wave reflections on the nozzle plate. This cannot be the source of the single burst observed for the incompressible flow since the latter is not subjected to acoustic propagation and reflections. Intuitively, one would expect an increase rather than the observed decrease, in meniscus deceleration during *TZ4* and *TZ5* due to the backwards motion of the pze (cf. Fig. 2). Initially, we attributed this acceleration surge to surface tension forces arising from the inclination towards detachment of the drop as the free surface area is increased by the forward motion of the meniscus. Yet, solving the same problem excluding surface tension forces from the model resulted in qualitatively similar behavior, ruling out surface tension as the source of acceleration surge in incompressible flow.

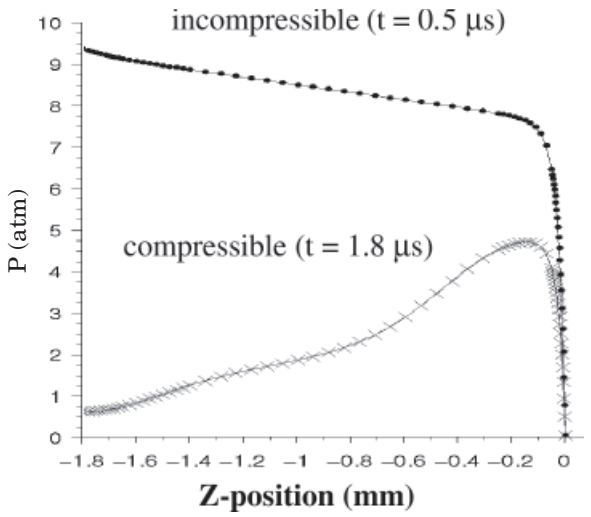

Figure 9. The axial pressure distribution along the symmetry axis upon reaching the highest pressure value in the system. Comparison between the compressible (t = 1.8 μs, within *TZ3*) and incompressible (t = 0.5 μs, within *TZ1*) flows.

The physical mechanism responsible for this feature was finally identified[8] as the flow of ink into the ink chamber through the porous wall during the backward motion of the pze during *TZ4* and *TZ5*.

The pressure profile curves along the symmetry axis at the corresponding times at which the maximum pressure value has been attained for each flow model are shown in Fig. 9. The largest pressure magnitudes are observed at t = 1.8 μs (*TZ3*) and t = 0.5 μs (*TZ1*) for the compressible and incompressible flows, respectively. Since as indicated in Fig. 9, the largest pressure in the incompressible flow is considerably larger than that for compressible flow it is natural to expect correspondingly higher meniscus velocity and acceleration in the former. Yet, Fig. 6 shows a slightly larger meniscus velocity for the compressible flow and although the maximum acceleration of the incompressible meniscus tip is higher than that of the compressible flow (Fig. 7), the difference does not reflect the large difference in pressure values (Fig. 9). This discrepancy is attributed to the short lived increase and decrease of the pressure in the case of incompressible flow, as opposed to the relatively slow pressure reflection at the nozzle exit section in the compressible flow.[8]

Finally, the flow reversal in the tapered section of the nozzle discussed at the end of the previous section, can give rise to instabilities which, in turn, may contribute to the formation of satellite droplets due to its close proximity to the forming drop. The finding that flow reversal is independent of liquid compressibility leads to the surprising conclusion that this important drop formation flow feature is not acoustically driven.

Conclusions

A numerical investigation comparing compressible and incompressible flow models was undertaken in order to examine the importance of ink compressibility in DOD nozzle internal operation and drop formation. The maximum pressure generated in the incompressible flow is 10 atm adjacent to the pze wall. The resulting relative change in density is extremely small on the order of 5×10^{-4}. Nevertheless, the very-slightly-compressible flow and the incompressible flow are very different in many aspects of the flow and drop evolution characteristics.

It is concluded that acoustic effects cannot be ignored in this flow system despite the low Mach number and the small condensation. The propagation of pressure along the ink chamber cannot be considered instantaneous relative to the fast motion of the pze wall. Thus, the incorporation of ink compressibility in the physical analysis of this flow system is essential. It should be noted that in some instances it may prove useful to examine as well, specific flow features in the absence of compressibility as a way to determine whether acoustic effects are responsible for that feature. The reversal of the flow field near the nozzle exit may serve as an example in which this type of comparison was employed, leading to the important finding that acoustic phenomena were not responsible for it.

Acknowledgment. We thank Prof. Jonatan Wachtel and Mr. Haggai Karlinski from "Aprion Digital" for many fruitful discussions and for sharing their knowledge with us. We are grateful for the financial support provided by the DPI Magnet program established by Israel Ministry of Industry and Trade. Publication expenses have been funded by the Reimund Stadler Minerva Center for Mesoscale Macromolecular Engineering. Minerva is funded through the BMBF.

References

1. J. D. Beasley, Model for fluid ejection and refill in an impulse drive jet, *Photogr. Sci. Eng.* **21,** 78 (1977).
2. J. Q. Feng, A general fluid dynamic analysis of drop ejection in drop-on-demand jet devices, *J. Imaging Sci. Technol.* **46,** 398 (2002).
3. D. E. Bogy and F. E. Talke, Experimental and theoretical study of wave propagation phenomena in drop-on-demand ink jet devices, *IBM J. Res. Dev.* **28,** 314 (1984).
4. T. W. Shield, D. E. Bogy and F. E. Talke, Drop formation by DOD ink jet nozzle: A comparison of experimental and theoretical simulation, *IBM J. Res. Dev.* **31,** 96 (1987).
5. C. Ping-Hei, P. Hsin-Yah, L. Hsin-Yi, S. L. Chang, T. I. Wu, and C. Chiang-Ho, Pressure response and droplet ejection of a piezoelectric inkjet printhead, *Int'l. J. Mech. Sci.* **41,** 235 (1999).
6. B. V. Antohe and D. B. Wallace, Acoustic phenomena in a demand mode piezoelectric ink jet printer, *J. Imaging Sci. Technol.* **46,** 409 (2002).
7. G. Strang and G. J. Fix, *An Analysis of the Finite Element Method*, Prentice-Hall, Englewood Cliffs, N.J., 1973.
8. E. Magen and M. Gottlieb, Pressure distribution and flow field inside a DOD piezoelectric ink jet nozzle, *J. Imaging Sci. Technol.* in press.
9. E. Magen, *CFD simulations of the flow inside a piezoelectric ink jet nozzle*, M.Sc. Thesis, Ben Gurion Univ., Beer Sheva, Israel, 2003.
10. H. Karlinski and J. Wachtel, Aprion Digital, personal communication, 2001.
11. L. E. Kinsler, A. R. Frey, A. B. Coppens, and J. V. Sanders, *Fundamentals of Acoustics*, 3rd ed., John Wiley and Sons, New York, 1982.
12. R. B. Bird, W. E. Stewart, and E. N. Lightfoot, *Transport Phenomena*, John Wiley and Sons, New York, 2002.
13. *Polyflow User Manual*, Version 3.6.0, Louvain-La-Neuve, Belgium, 1998.
14. L. D. Landau and E. M. Lipshitz, *Fluid Mechanics*, Pengamon Press, Oxford, 1959, pp. 24, for an alternative discussion of this issue.